Preparation of Lignin-based Mesoporous Biochar Nano- and Microparticles, and Their Adsorption Properties for Hexavalent Chromium

Yu Hu,[#] Meng Ling,[#] and Xianfa Li *

The removal performance and mechanism of Cr(VI) from aqueous solution was studied for a novel micro-nano particle kraft lignin biochar (BC) pyrolyzed at 400 to 700 °C. The physicochemical properties of BC were determined by Fourier transform infrared spectroscopy (FTIR), scanning electron microscopy (SEM), and N_2 adsorption-desorption isotherms. The results illustrated that the BC had irregular micro- and nanoparticles with abundant pore structure and high BET surface area (111.1 m^2/g). The FT-IR results showed that the lower pyrolysis temperature resulted in more oxygen-containing functional groups. The Cr(VI) adsorption capacity decreased with the pyrolysis temperature increasing from 400 to 700 °C, and the maximum percentage removal of Cr(VI) for BC obtained at 400 °C was 100% at pH 2, which suggested that the removal efficiency was mainly dependent on functional groups. Kinetic analysis demonstrated that Cr(VI) adsorption on BC fit well to the pseudo-second-order kinetic model. The adsorption data was well fitted with the Langmuir isotherm models, and the maximum adsorption capacity was 37.2 mg/g at 298K. The BC could be reused twice with Cr(VI) removal of 63.91% and was suitable for Cr(VI) contaminated waste-water treatment.

Keywords: Industrial kraft lignin; Biochar; Cr(VI); Adsorption mechanism

Contact information: School of Life Science and Engineering, Southwest University of Science and Technology, Mianyang 621010, China; #These authors contributed equally;
** Corresponding author: lixianfa@swust.edu.cn*

INTRODUCTION

Heavy metals enter bodies of water through manufacturing, smelting electroplating activities, and improper use of chemical fertilizers and pesticides in agriculture, leading to serious water pollution (Zhang *et al.* 2018). Heavy metals cannot be degraded. Once they are absorbed by the human body, they are difficult to be metabolized and discharged, causing poisoning and even endangering life (Yang *et al.* 2020). In particular, Cr(VI) has serious carcinogenicity, toxicity, and strong mobility, so it is a serious threat to human health. Long-term exposure to Cr(VI) may cause damage to the respiratory tract, skin, eyes, gastrointestinal tract, *etc*., and it can cause dermatitis, eczema, cancer, and even death (Wang *et al.* 2013; Sehrish *et al.* 2019; Wang *et al.* 2019).

Various methods have been applied to remove Cr(VI) from wastewater, such as precipitation, reverse osmosis, and adsorption (Lu *et al.* 2018; Yang *et al.* 2018). Among the above methods, adsorption has the advantages of environmental friendliness, easy operation, low cost, wide adaptability, and easy recyclability. Adsorbents such as chitosan, zeolite, agroforestry waste, activated carbon and grapheme are widely applied in Cr(VI) wastewater treatment (Ali *et al.* 2012; Shen *et al.* 2012; Zibaei *et al.* 2020). Although chitosan has strong adsorption performance, it has small specific surface area, high cost,

and poor mechanical and thermal properties. Agricultural and forestry wastes, such as straw, fruit shells, and sawdust, come from a wide range of sources; they are cheap, renewable, easy to obtain, and have little secondary pollution. However, they contain fewer active functional groups on the surface and have poor adsorption performance. Although zeolites, activated carbon and graphene have large specific surface area and have a wide range of applications in environmental pollution treatment, these adsorbents exhibit easy blockage of pores, high cost, and difficult recovery after utilization (Yousef *et al*. 2011; Demarchi *et al*. 2019).

Biochar (BC) has promising adsorption performance in Cr(VI) wastewater treatment due to its high specific surface area, porous structure, high cation exchange capacity (CEC), abundance of functional groups, negative charges, and good stability (Shibo *et al.* 2017). Some studies have shown that BC has good application performance for Cr(VI) removal in wastewater. Khali *et al.* (2020) found that maximum percentages of 99.3% and 96.8% Cr(VI) were removed by tea waste and rice husk biochar at pH 5.2, respectively. The functional groups such as hydroxyl (-OH) and carboxyl (-COOH) promote the reduction of Cr(VI) to Cr(III) on the surface of BC (Reddad *et al.* 2003; Liang *et al.* 2014). Moreover, biochar not only can provide electrons for the reduction of Cr(VI) through surface oxygen-containing functional groups (*e.g*. C=O), but also it can act as an electron shuttle during the reduction of Cr(VI), resulting in more Cr(VI) being removed (Liu *et al.* 2020). BC has been prepared from various plants and animal manure, such rice hull (Liu *et al.* 2019), cotton stalk (Tariq *et al.* 2020), tea residue (Khalil *et al.* 2020), peanut husk (Wang *et al.* 2019), pig manure (Duan *et al.* 2017), *etc*. However, it is still necessary to find waste biomass materials with low cost, easily availability, and high adsorption capacity to be used as potential raw materials to prepare BC for Cr(VI) removal. Lignin is a potential material for BC production, as it is a renewable natural polyphenolic polymer, the second richest waste biomass after cellulose.

Approximately 50 million tons of industrial lignin are produced per year in the paper and pulping industries (Naseer *et al.* 2018). Part of industrial lignin is discharged directly as black liquor, which wastes resources and causes environmental pollution. The traditional method is to condense and burn black liquor to recover the heat (Masashi *et al*. 2011). The preparation of BC is an effective way to solve lignin resource utilization and environmental pollution. Mesoporous BC has a large specific surface area and pore volume, which is beneficial to the adsorption and fixation of heavy metal ions (Wang *et al.* 2019).

In this work, industrial kraft lignin isolated by CO_2 precipitation and sulfuric acidification from paper and pulping black liquor was applied to prepare mesoporous micro-nano BC by pyrolysis at 400 to 700 ℃, and the physicochemical properties such as functional groups, morphology, and structure of BC were tested with Fourier transform infrared spectroscopy (FT-IR), scanning electron microscopy (SEM), X-ray diffraction (XRD), N_2 adsorption-desorption, and nanoparticle size analysis. Batch adsorption experiments and the effect of solution pH and BC dosage were investigated. Adsorption isotherm and kinetics were applied to reveal the mechanism of Cr(VI) adsorption. This work provides a novel, cheap, efficient, and green adsorption material for Cr(VI) removal, as well as an effective approach for industrial waste utilization.

EXPERIMENTAL

Materials

Potassium dichromate ($Cr_2K_2O_7$), hydrochloric acid (HCl), and sodium hydroxide (NaOH) were analytically pure and purchased from Chengdu Kelong Chemical Co., Ltd. (Chengdu, China). Industrial kraft lignin was purchased from the Xuemei Paper mill in Shandong province (Shandong, China).

BC Preparation

The industrial kraft lignin was placed in a porcelain crucible with a lid to create a limited oxygen environment and pyrolyzed in the muffle furnace (SX-5-12; Tianjin Tester Instrument Co., Ltd., Tianjin, China) at 400, 500, 600, or 700 ℃, respectively. The limited oxygen pyrolysis lasted for 2 h, followed by cooling to room temperature. After cooling, the BC was washed with deionized water to remove soluble impurities and then oven-dried overnight at 60 ℃. According to the different pyrolysis temperatures, the BC were named as BC400, BC500, BC600, and BC700.

Methods

Characterization of BC

The specific surface area and pore parameters of BC were measured using an AutOSORbon-1MP device (Quantachrome, Boynton Beach, FL, USA) at 77 K. Before the analysis, the sample was degassed under vacuum at 350 K for 6 h. The particle size of BC was determined by nano particle size analyzer (90PLUS; Brookhaven, New York, USA). The morphology of BC was characterized using a scanning electron microscope (SEM; UItra55; Carl Zeiss NTS GmbH, Oberkochen, Germany). The surface functional groups of BC were determined by inspecting Fourier transform infrared spectra (FT-IR) (Spectrum One; PerkinElmer, Waltham, MA, USA). The pH of BC was determined using a pH meter with carbon-water ratio of 1:20. The Ash content of BC was determined using a standard method (GB/T176641999).

Batch adsorption experiments

A standard stock solution (Cr(VI) 1000 mg/L) was prepared by dissolving $Cr_2K_2O_7$ in ultrapure water, then the stock solutions were diluted to 30-180 mg/L Cr(VI) solutions. In the adsorption experiments, to investigate the effect of pH and pyrolysis temperature on Cr(VI) removal efficiency, 0.2 g BC was added into the conical flask with the Cr(VI) solution (50 ml, 50 mg/L) with the pH-adjustment of 1 to 9 by using either 1 mol/L HCl or NaOH. Stirring with a constant speed of 150 r/min and contact time of 24 h with temperature 298 K were applied. The adsorption capacity of Cr(VI) (q_t) and removal efficiency (R_e) were calculated by Eqs.1 and 2, respectively,

$$q_t = (C_0 - C_t)V/m \quad (1)$$

$$R_e = (C_t - C_0)/C_0 \times 100\% \quad (2)$$

where C_0 and C_t(mg/L) are the Cr(VI) concentration in solution at the initial and at time t (h), respectively, V(L) is simulated waste-water volume, and m(g) is mass of BC.

The optimum pH and carbonization temperature were achieved during the above

experiments. On this basis, the effects of BC400 dose (0.1 to 0.4 g), initial concentration (30 to 180 mg/L), contact time (0 to 24 h), and temperature (288 to 318 K) on the adsorption of Cr(VI) were observed.

Regeneration and reutilization experiments

The recyclability of BC400 on the corresponding optimum Cr(VI) solution concentration, reaction time, and pH were studied. After adsorption equilibrium, the mixtures were vacuum filtered through a 0.45 μm membrane, and the spent BC400 was dried after washing with deionized water to remove any unabsorbed metal ions. The spent BC was desorbed with 0.1 mol/L NaOH and reused.

Adsorption Isotherm, Kinetic, and Thermodynamic Model

Adsorption isotherm

The adsorption isotherm indicates adsorption equilibrium relationship between the Cr(VI) adsorbed onto BC and the Cr(VI) in solution, which is represented by the Langmuir (Eq. 3), Freundlich (Eq. 4), and Temkin (Eq. 5) equations (Liu *et al.* 2020),

$$C_e/q_e = 1/K_L q_m + C_e/q_m \quad (3)$$

$$q_e = K_F C_e^{1/n} \quad (4)$$

$$q_e = RT/b_T \ln k_T + RT/b_T \ln C_e \quad (5)$$

where C_e (mg·L^{-1}) is equilibrium concentration, q_e(mg·g^{-1}) and q_m (mg·g^{-1}) are the adsorption equilibrium capacity and maximum adsorption capacity, respectively. K_L (mg·L^{-1}) and K_F [(mg·g^{-1})·(mg·L^{-1})$^{-n}$] are Langmuir and Freundlich model parameters, respectively. The parameter n is adsorption intensity, R is the universal gas constant, 8.314 J/mol·k, and k_T (L·mg^{-1}) and b_T(J·mol^{-1}) are Temkin characteristic constants.

The Langmuir model assumed that the surface of adsorbent has just one class of non-interacting sites of adsorption. The Freundlich isothermal model suggested that adsorption is a multilayer adsorption on the heterogeneous surface. The Temkin isothermal model assumed that a linear relationship between adsorption heat and temperature to judge chemical adsorption or physical adsorption.

Adsorption kinetics

The adsorption kinetics of Cr(VI) onto BC was described by pseudo-first order (PFO), pseudo-second order (PSO), intra-particle diffusion (IPD), and Elovich models, as shown in Eqs. 6 through 9, respectively (Wang *et al.* 2019),

$$ln(q_e - q_t) = ln\, q_e - K_1 t \quad (6)$$

$$t/q_t = 1/K_2 q_e^2 + t/q_e \quad (7)$$

$$q_t = K_3 t^{0.5} + b \quad (8)$$

$$q_t = 1/\beta \ln(\alpha\beta) + 1/\beta \ln t \quad (9)$$

where q_e (mg·g^{-1}) and q_t(mg·g^{-1}) are the amount of adsorbed Cr(VI) at equilibrium and at time t (h), respectively. The parameters k_1 [g·(mg·h)$^{-1}$], k_2 [g·(mg·h)$^{-1}$] and k_3 [mg·(g·min$^{-0.5}$)$^{-1}$] are the rate constants for PFO, PSO, and IPD, respectively. The parameter α (mg·h^{-1})

is the initial removal rate, and β ($g \cdot mg^{-1}$) is the desorption coefficient.

Thermodynamic model

The thermodynamic process of Cr(VI) adsorption on BC was studied by the thermodynamic parameters including ΔG^0, ΔH^0, and ΔS^0. The change in free energy ΔG^0 is calculated from Eqs.10 and 11; ΔH^0 and ΔS^0 can be obtained by the slope and the intercept of the plot of $\ln K_d$ *versus* $1/T$, respectively (Eq. 12),

$$\Delta G^0 = -RT \ln K_d \quad (10)$$

$$K_d = {}^{q_e}/_{C_e} {}^{W}/_{V} \quad (11)$$

$$\Delta G^0 = \Delta H^0 - T\Delta S^0 \quad (12)$$

where T(K) is initial temperature, R is the ideal gas constant, 8.314 J/mol·k, K_d is the adsorption partition coefficient, and V(L) is the simulated waste-water volume.

Data Analysis

The concentration of Cr(VI) was measured using a visible spectrophotometer (WFJ7200; Shanghai, China) at 540 nm with the 1,5 diphenyl carbazide method (Wang *et al.* 2019). All experimental data were repeated in triplicate, and the mean value was taken as the measurement result. Microsoft Excel2019 (Redmond, WA, USA) was used for statistical analysis. Figures were drawn with OriginPro 8.0 (Northampton, MA, USA).

RESULTS AND DISCUSSION

Characterization of BC

Physical and chemical properties of kraft lignin and BC

The physicochemical properties of kraft lignin and BC obtained at different temperatures are shown in Table 1. Kraft lignin was found to be an idea precursor for BC preparation, since it had high C content (54.9%) and low ash content (5.11%) and the content of C and ash rose with increasing pyrolysis temperature after carbonization. BC yield rapidly decreased (60.6 to 53.8%) with increasing pyrolysis temperature from 400 to 500 ℃, which is due to some carbon-containing components decomposing into liquid and gas (Liu *et al.* 2017). However, the decrease is not obvious (49.5 to 46.5%) at high temperatures (from 600 to 700 ℃), which indicates that most volatile components had been lost at relatively low temperature. The ash content increased from 6.99 to 10.02% with pyrolysis temperature increasing from 400 to 600 ℃, indicating that most inorganic components accumulated in BC during pyrolysis. The ash content did not change significantly with the increase of temperature, suggesting that the carbonization process tends to stabilize. In this study, the ash content of BC was obviously lower than that of most reported plant BC (Shinogi and Kanri 2003; Wang *et al.* 2018). The pyrolysis temperature has a high impact on the pH of BC. With the pyrolysis temperature rising from 400 to 700 ℃, the pH value increased from 4.60 to 7.62, which was attributed to fewer surface acidic functional groups and more ash content of BC obtained at higher carbonization temperature. The result was consistent with the ash content change.

Table 1. Physical and Chemical Properties of Kraft Lignin and BC at Different Pyrolysis Temperatures

Sample			Proximate Analysis (%)				Ultimate Analysis (%)			
	Yield	pH (1:20)	Moisture	Fixed carbon	Volatile matter	Ash	C	H	N	O
Kraft lignin	-	-	9.26	39.84	45.79	5.11	54.91	4.94	0.93	30.78
BC400	60.59	4.81	2.25	71.38	19.38	6.99	68.05	2.45	1.45	20.69
BC500	53.80	5.67	2.05	73.13	16.34	8.48	73.81	3.06	1.39	12.71
BC600	49.47	6.93	2.00	76.85	11.13	10.02	73.33	3.45	1.16	11.45
BC700	46.50	7.62	1.65	81.08	6.55	10.72	77.91	2.05	1.01	7.61

The FT-IR spectra of BC are shown in Fig. 1. Figure 1(a) shows that with the increasing pyrolysis temperature, the intensity of hydroxyl (-OH) stretching peak vibration at 3432 cm^{-1} decreased due to the dehydration reaction increasing in BC (Chen *et al.* 2020). The band with peaks at 2921 and 2852 cm^{-1} are assigned to C-H deformation vibration with the alkanes functional groups (methyl-CH_3, methylene-CH_2), and the intensity decreased with increasing pyrolysis temperature, which indicates that the aliphatic functional group structure and the surface polarity decreased in BC (Wang *et al.* 2019). The absorbance peak at 1705 cm^{-1} corresponds to the stretching vibration of the -COOH groups, which led to the reduction of functional groups as the pyrolysis temperature was increased. The peaks at 1628 cm^{-1} were attributed to C-O and aromatic C-C stretching vibration, which is gradually diminished with the increase of pyrolysis temperature (Jiang *et al.* 2019). The absorption peak at 1048 cm-1 corresponds to C-H of guaiac based aromatic group in-plane vibration (Maldhure and Ekhe 2011). In addition, the peak ascribed to bending vibrations of the benzene ring at 879 cm^{-1} disappeared with increasing temperature, which indicates that the increase of pyrolysis temperature may enhance the aromatization of BC. The spectra after BC400 adsorption Cr(VI) is shown in Fig. 1(b). Cr(VI) was adsorbed onto BC400, and an obvious shift migration was observed in this functional group peaks including -OH, C=O, and -COOH. The results indicate that the functional groups on the surface of BC were involved in the adsorption of Cr(VI).

At 400 ℃, the BC yield was the highest, with low ash content, and abundant surface oxygen functional groups. The optimum pyrolysis temperature of 400 ℃ was selected and used for subsequent characterization.

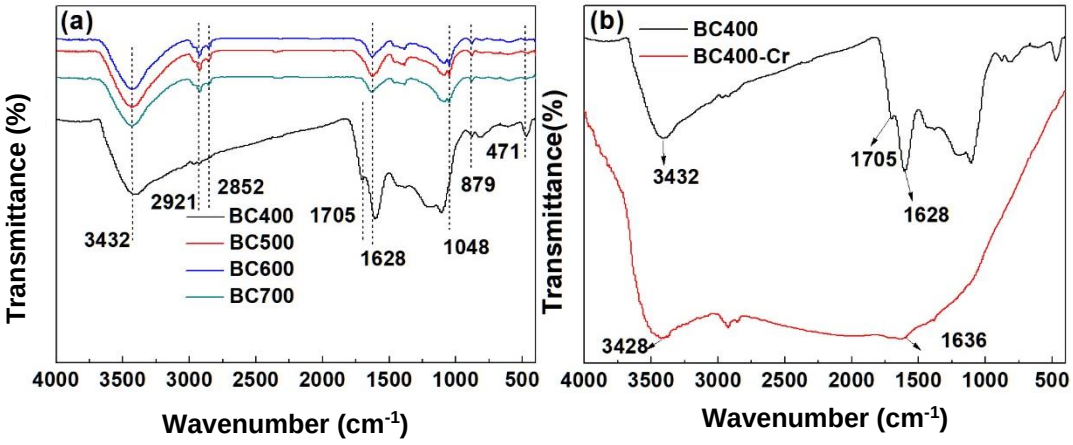

Fig. 1. FT-IR of BC obtained from various carbonization temperature (a) and BC400 (b) before and after adsorption

The morphology of BC400 was imaged by SEM. As shown in Fig. 2a, the size of BC400 particles was mostly in micro-nanometer scale, and all particles were within 8 microns. The surface is rough, and shape is very irregular. A lot of macroporous and super macroporous particles were observed (Fig. 2b), which constitute a high specific surface area of BC400.

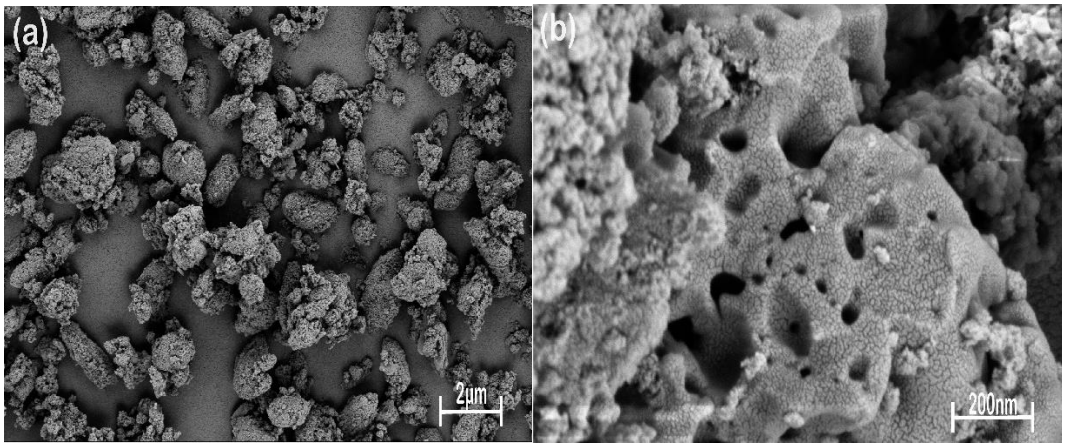

Fig. 2. SEM diagram of BC400with two different magnifications(a)at 2kx (b)at 40kx

The specific surface area and pore size distribution of BC400 were analyzed by N_2 adsorption, and the results are shown in Fig. 3. The adsorption-desorption isotherms and the hysteresis loop can be categorized as type IV and H_3, respectively, according to the IUPAC classification. The adsorption hysteresis is related to the size and shape of pores (Kondo *et al.* 2005). The N_2 adsorption-desorption isotherms of BC400 were not closed at very low relative pressure (P/P_0 < 0.3), indicating abundant microporous structures inBC400. With increased relative pressure, the amount of adsorption N_2 onto BC400 was enhanced steadily in the medium relative pressure range (P/P_0 = 0.3 to 0.8) and produced multi-layer adsorption, indicating that there were many mesopores. As the pressure was raised to the high relative pressure (P/P_0 = 0.9 to 1.0), the amount of adsorption increased sharply, demonstrating the existence of certain number of macropores.

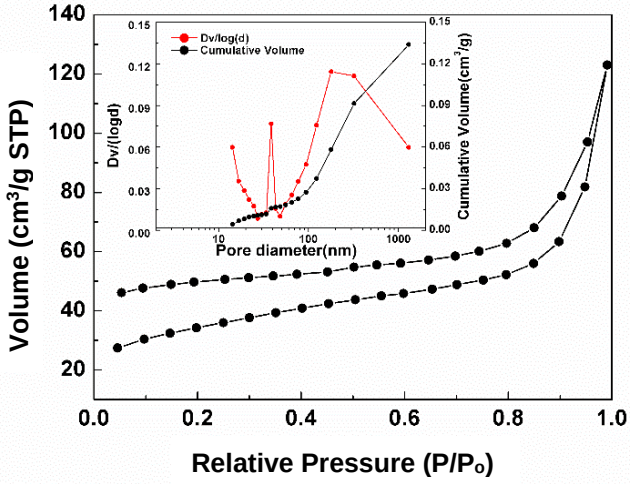

Fig. 3. N_2 Adsorption - desorption isotherm and pore size distribution of BC400

The pore size distribution curve of BC400 is shown in Fig. 3. It was calculated from the BJH model. As can be seen, the peak of BC400 centered at 38.4 nm, and the broad peak also appear at 178.3 to 320.8 nm, indicating that the BC400 had a porous structure with mainly mesopores and macropores, which is also demonstrated by the cumulative distribution curve of pore size. BC400 had a higher specific surface area (111.10 m^2/g) compared with other biochars, such as sugarcane bagasse (92.3 m^2/g) and hardwood (5.6 m^2/g) derived BC, which can provide the abundant active sites for the subsequent Cr(VI) adsorption (Lahori *et al.* 2017). Many mesopores facilitate Cr(VI) migration to the adsorption sites and improve the adsorption performance of BC400 (Chen *et al.* 2020). Thus, BC400 demonstrated good performance for the removal of Cr(VI), as shown in the experiments below.

A smaller particle size sometimes results in a larger specific surface area and stronger adsorption of Cr(VI) (Khiari *et al.* 2020). The average particle size and particle size distribution of BC were measured by nanoparticle size analyzer through the suspension method. Figure 4 shows the particle size distribution map of BC400, in which the particle size is concentrated in the range of 259.9 to 274.4 nm, with an average of 267.7 nm. The result suggests that BC400 particles are nanoscale with a large specific surface area, which is consistent with the analysis results of specific surface area.

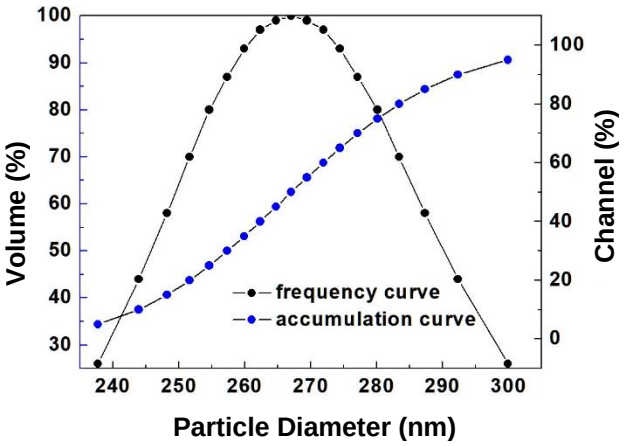

Fig. 4. Grain size distribution curve of BC400

Effect of pH and BC400 dosage

The effect of pH on Cr(VI) adsorption is shown in Fig. 5a. As the pyrolysis temperature was increased from 400 to 700 °C, the adsorption capacity of BC obviously decreased with increasing pH. At pH 2, $HCrO_4^-$ is the dominant species of Cr(VI) (Liang *et al.* 2014). $Cr_2O_7^{2-}$ and $HCrO_4^-$ are major species from pH 2 to 6, and the ionic radius of $Cr_2O_7^{2-}$ is larger than that of the $HCrO_4^-$. The $HCrO_4^-$ is easier to diffuse in the solution, which is beneficial to adsorption (Shan *et al.* 2020). With the increase of pH, CrO_4^{2-} is the main species of Cr(VI) in solution. As the content of OH^- increases, there will be competitive adsorption between CrO_4^{2-} and OH^-, which further decreased the adsorption capacity (Lu *et al.* 2019). However, the adsorption capacity decreased slightly with the increase of carbonization temperature, indicating that the surface oxygen-containing functional groups may influence the removal of Cr(VI). Therefore, pH 2 and a pyrolysis temperature of 400 °C were selected for the subsequent experiments.

BC dosage is an important factor to influence the adsorption efficiency. As shown

in Fig. 5b, with the increase of the BC400 dosage from 1 to 3 g/L, the removal percentage of Cr(VI) increased rapidly from 67.3 to 100%. This result shows that when the adsorption process is close the equilibrium, the increase of the BC400 dosage has little significance. However, the adsorption amount of BC400 to Cr(VI) on per unit weight decreased continuously with increasing dosage of BC400, as shown in Fig. 5b.

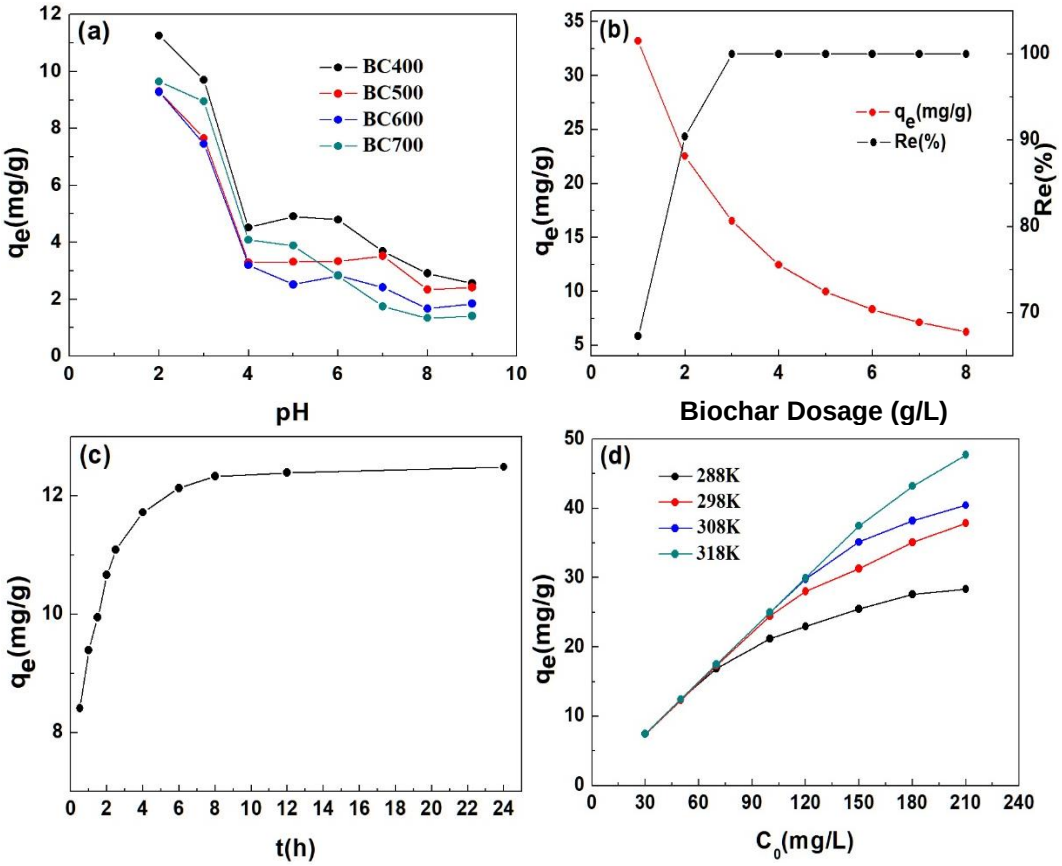

Fig. 5. (a) Effect of pH on the adsorption amount of Cr(VI) (adsorbent doses= 4 g/L, 50 mg/L, 25 °C, 150 r/min); (b) Effect of BC400 dosage on adsorption Cr(VI) (pH=2, 50 mg/L, 25 °C, 150 r/min); (c) Effect of contact time on the adsorption Cr(VI) of BC400 (BC400 doses= 4 g/L, 50 mg/L, 25 °C, 150 r/min); (d) Adsorption isotherm of Cr(VI) on BC400. (BC doses= 4 g/L, pH=2, 150 r/min).

Adsorption kinetics

The effect of contact time on Cr(VI) adsorption by BC400 is shown in Fig. 5c. In the initial stage the absorption rate increased rapidly within contact time from 0 to 2.5 h, and it reached equilibrium at 8 h. This can be mainly attributed to a large number of active sites in the initial stage of adsorption on the surface of BC400. In the second stage, the external active sites of BC400 gradually tended to be saturated, and the adsorption was probably limited by forces between the solute molecules of the solid and bulk phase, making it difficult for Cr to occupy the remaining adsorption sites (Liang *et al.* 2014).

The pseudo-first-order, pseudo-second-order, Elovich, and intra-particle diffusion models were used to fit the experimental data. The plots of the kinetic model are shown in supplementary data. The plots of kinetic model are shown in Fig. S1, and the fitting parameters are tabulated in Table 2. Compared with the pseudo-first-order kinetic model (R^2=0.955), the coefficient of determination (R^2=0.999) of the pseudo-second-order kinetic

model was closer to 1. The result indicated that Cr(VI) adsorption process on BC400 is more suitable for the pseudo-second-order kinetic model, and the adsorption process is limited by diffusion phenomena (Hubbe *et al*. 2019). The R^2 (0.972) value of the Elovich model was close to 1, which indicates that the Cr(VI) adsorption may involve a multiphase or multi-mechanism adsorption process (Dai *et al.* 2018). To further understand the rate-limiting steps, the experimental data were fitted by the intra-particle diffusion model. The fitting curve for BC400 adsorption Cr(VI) was multi-linear, such that the adsorption process is divided into two stage. The corresponding parameters are listed in Table 2, which shows that the adsorption rate $K_{i,1} > K_{i,2}$. At the first stage, Cr(VI) was absorbed rapidly to the surface of BC400 mainly through film diffusion. In the second stage, the Cr(VI) moved from the exterior surface of the BC400 to the internal structure. As the Cr(VI) diffused into the pores, the diffusion rate decreased due to the increase of diffusion resistance. The fitting curve deviates the origin, which indicates that the adsorption process of BC400 adsorption Cr(VI) is controlled by both external and intra-particle diffusion.

Table 2. Cr(VI) Adsorption Kinetic Model Parameter Fitting

PFO			PSO		
q_e (mg g^{-1})	k_1	R^2	q_e (mg g^{-1})	K_2	R^2
3.636	0.345	0.955	12.807	0.212	0.999
IPD					
$K_{i,1}$	C_1 (mg L^{-1})	R_1^2	$K_{i,2}$	C_2 (mg L^{-1})	R_2^2
2.704	6.592	0.971	0.253	11.542	0.674
Elovich model					
α		R^2		β	
9.321		0.972		0.493	

Adsorption isotherm

The adsorption rate of Cr(VI) as a function of concentration at equilibrium at various temperature is shown in Fig. 5d. The Langmuir, Freundlich, and Temkin isothermal adsorption models were used to fit the equilibrium data. The related parameters are summarized in Table 3. The R^2 (0.993) of Langmuir isotherm was closer to 1 than that of Freundlich model (0.876), which indicates that the Langmuir isotherm fitted better than the Freundlich isotherm, and the Cr(VI) adsorption of BC400 can be modeled based on an assumption of equal-energy, non-interacting adsorption sites (Lalvani *et al.* 1997; Jiang *et al.* 2019). The Temkin model also had a relatively high R^2 value (0.968), indicating that the adsorption process of the Cr(VI) can be also described by Temkin model.

Table 3. Adsorption Isothermal Parameter of Cr(VI) on BC

Model	Langmuir			Freundlich			Temkin		
	q_{max} (mg g^{-1})	k_L	R^2	1/n	k_F	R^2	b_T	k_T	R^2
288K	28.4	0.375	0.994	0.144	7.299	0.943	1018.526	18.842	0.958
298K	37.2	0.916	0.993	0.168	8.125	0.876	735.246	18.286	0.968
308K	40.1	2.746	0.998	0.154	8.674	0.631	733.672	21.416	0.823
318K	47.5	8.195	0.998	0.160	9.411	0.351	614.854	22.591	0.570

Adsorption thermodynamics

The effect of temperature on Cr(VI) adsorption of BC was investigated within a temperature range ranging from 288 to 318K. The results also are shown in Fig. 5d. The

adsorption capacity of Cr(VI) rose with the increase of temperature, indicating that the Cr(VI) adsorption on BC400 is an endothermic (Zhang *et al*. 2017). The higher temperature is favorable to create more adsorption site onto BC400.

The thermodynamic parameters obtained from Eqs. 8 and 9 are shown in Table 4. ΔG^0 had a negative value that decreased with the increase of temperature, indicating that the adsorption reaction was spontaneous. In addition, ΔH^0 and ΔS^0 were positive, indicating that the adsorption of Cr(VI) onto BC400 was endothermic, and the adsorption of Cr(VI) onto BC400 had good affinity.

Table 4. Cr(VI) Adsorption Thermodynamic Parameters

ΔH^0 (kJ·mol^{-1})	ΔS^0 (J·mol^{-1})	ΔG^0 (kJ·mol^{-1})			
		288K	298K	308K	318K
21.053	0.129	-15.381	-18.298	-18.751	-19.525

Regeneration and Reutilization of BC400

The regeneration and reutilization of BC400 was determined at optimized conditions (Cr(VI)ions concentration 70 mg/L, pH 2, contact time 12 h). After use, the spent BC400 was filtered and regenerated by shaking with 0.1 mol/L NaOH aqueous solution. The regeneration was repeated twice. The removal percentage of Cr(VI) decreased obviously, but it still reached 63.9% after the third utilization (Fig. 6). The results revealed that BC400 showed reusability and stability for the decontamination of Cr (VI) contaminated water.

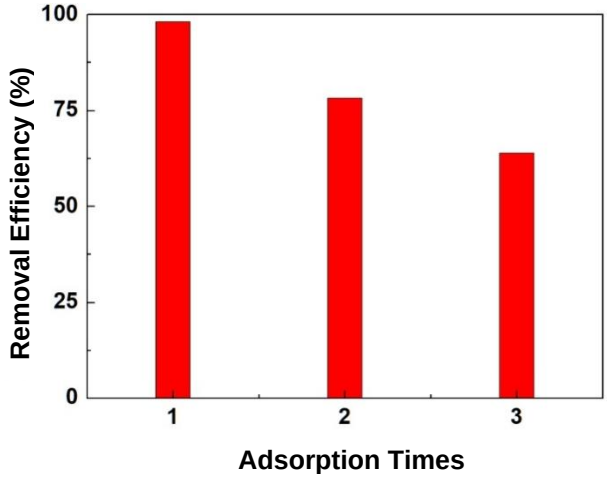

Fig. 6. Removal rate of Cr(VI) for BC400 in multiple adsorption-regeneration cycles

CONCLUSIONS

1. A novel mesoporous micro-nano BC prepared from industrial kraft lignin was used to remove of Cr(VI) from wastewater. The BC particles had a mean diameter of 268 nm and high surface area (111.1m^2/g), which was beneficial for Cr(VI) adsorption.
2. The effect of pyrolysis temperature, pH, and contact time were optimized. The results showed that optimum value of pyrolysis temperatures and pH for removal of Cr(VI)

were 400 ℃ and pH 2, respectively.

3. Adsorption of Cr(VI) could be fitted well to the pseudo-second-order kinetics model. Langmuir isotherm model best explained the Cr(VI) adsorption data, with the maximum adsorption capacity of 37.2 mg/g at 298 K. The thermodynamic result showed the adsorption of Cr(VI) was spontaneous and endothermic. Regeneration experiments further suggested that BC400 can be reused in Cr(VI) wastewater treatment.

ACKNOWLEDGMENTS

This work was supported by the Key Research and Development Plan of the Science & Technology Department of Sichuan Province (2018SZ0301).

REFERENCES CITED

Ali, I., Thabet, M., El-Nasser, K. S., Hassan, A. M., and Salama, T. (2012). "Synthesis of nanosized ZSM-5 zeolite from rice straw using lignin as a template: Surface-modified zeolite with quaternary ammonium cation for removal of chromium from aqueous solution," *Microporous and Mesoporous Materials* 160, 97-105. DOI: 10.1016/j.micromeso.2012.04.020

Chen, Y. M., Chen, H. L., Thring, R. W., Liu, H., Zhou, J. M., Tao, Y. L., and Li, J. (2020). "Immobilization of chromium contaminated soil by co-pyrolysis with rice straw," *Water, Air, & Soil Pollution* 231(5), 1-13. DOI: 10.1007/s11270-020-04581-3

Dai, L., Zhu, W., He, L., Tan, F. R., Zhu, N. M., Zhou, Q., He, M. X., and Hu, G. (2018). "Calcium-rich biochar from crab shell: An unexpected super adsorbent for dye removal," *Bioresource Technology* 267, 510-516. DOI: 10.1016/j.biortech.2018.07.090

Demarchi, C. A., Michel, B. S., Nedelko, N., Ślawska-Waniewska, A., Dłużewski, P., Kaleta, A., Minikayev, R., Strachowski, T., Lipińska, L., Magro, J. D., and Rodrigues, C. A. (2019). "Preparation, characterization, and application of magnetic activated carbon from termite feces for the adsorption of Cr(VI) from aqueous solutions," *Powder Technology* 354, 432-441. DOI:10.1016/j.powtec.2019.06.020

Duan, S. B., Ma, W., Pan, Y. Z., Meng, F. Q., Yu, S. G., and Wu, L. (2017). "Synthesis of magnetic biochar from iron sludge for the enhancement of Cr(VI) removal from solution," *Journal of The Taiwan Institute of Chemical Engineers* 80, 835-841. DOI: 10.1016/j.jtice.2017.07.002

GB/T17664 (1999). "Wood charcoal and test method of wood charcoal," CSBTS (State Bureau of Quality Technical Supervision), Beijing, China.

Hubbe, M. A., Azizian, S., and Douven, S. (2019). "Implications of apparent pseudo-second-order adsorption kinetics onto cellulosic materials. A review," *BioResources* 14(3), 7582-7626. DOI: 10.15376/biores.14.3.7582-7626

Jiang, C., Bo, J., Xiao, X., Zhang, S., Wang, Z. H., Yan, G. P., Wu, Y. G., Wong, C. P, and He, H. (2019). "Converting waste lignin into nano-biochar as a renewable substitute of carbon black for reinforcing styrene-butadiene rubber," *Waste Management* 102, 732-742. DOI: 10.1016/j.wasman.2019.11.019

Khalil, U., Shakoor, M. B., Ali, S., Rizwan, M., Alyemeni, M. N., and Wijaya, L. (2020).

"Adsorption-reduction performance of tea waste and rice husk biochars for Cr(VI) elimination from wastewater," *Journal of Saudi Chemical Society* 24(11), 799-810. DOI: 10.1016/j.jscs.2020.07.001

Khiari, Z., Alka, K., Kelloway, S., Mason, B., and Savidov, N. (2020). "Integration of biochar filtration into aquaponics: Effects on particle size distribution and turbidity removal," *Agricultural Water Management* 229, article no. 105874. DOI: 10.1016/j.agwat.2019.105874

Kondo, S., Ishikawa, T., and Abe, I. (2005). *Adsorption Science*, Chemical Industry Press, Beijing, China.

Lahori, A. H., Guo, Z. Y., Zhang, Z. Q., Li, R. H., Mahar, A., Awasthi, M. K., Shen, F., Sial, T. A., Kumbhar, F., Wang, P., and Jiang, S. C. (2017). "Use of biochar as an amendment for remediation of heavy metal-contaminated soils: Prospects and challenges," *Pedosphere* 27(6), 991-1014. DOI:10.1016/s1002-0160(17)60490-9

Lalvani, S. B., Wiltowski, T. S., Murphy, D., and Lalvani, L. S. (1997). "Metal removal from process water by lignin," *Environmental Technology* 18(11), 1163-1168. DOI: 10.1080/09593331808616636

Liang, S., Guo, X. Y., Lautner, S., and Saake, B. (2014). "Removal of hexavalent chromium by different modified spruce bark adsorbents," *Journal of Wood Chemistry and Technology* 34 273-290.DOI: 10.1080/02773813.2013.869606

Liu, L. H., Liu, X., Wang, D. Q., Lin, H., and Huang, L. (2020). "Removal and reduction of Cr(VI) in simulated wastewater using magnetic biochar prepared by co-pyrolysis of nano-zero-valent iron and sewage sludge," *Journal of Cleaner Production* 257, article no. 120562. DOI: 10.1016/j.jclepro.2020.120562

Liu, X. Y., Yang, L., Zhao, H. T., and Wang, W. (2019). "Pyrolytic production of zero valent iron nanoparticles supported on rice husk-derived biochar: Simple, *in situ* synthesis and use for remediation of Cr(VI)-polluted soils," *The Science of the Total Environment* 708, article no. 134479. DOI: 10.1016/j.scitotenv.2019.134479

Liu, Y. X., Yao, S., Wang, Y. Y., Lu, H. H., Brar, S. K., and Yang, S. M. (2017). "Bio- and hydrochars from rice straw and pig manure: Inter-comparison," *Bioresource Technology* 235, 332-337. DOI: 10.1016/j.biortech.2017.03.103

Lu, H. P., Li, Z. A., Gasco, G., Méndez, A., Shen, Y., and Paz-Ferreiro, J. (2018). "Use of magnetic biochars for the immobilization of heavy metals in a multi-contaminated soil," *The Science of the Total Environment* 622-623, 892-899. DOI: 10.1016/j.scitotenv.2017.12.056

Lu, X. Q., Liu, X. W., Zhang, W. Q., Wang, X. H., Wang, S. G., and Xia, T. (2019). "The residue from the acidic concentrated lithium bromide treated crop residue as biochar to remove Cr (VI)," *Bioresource Technology* 296, article no. 122348. DOI: 10.1016/j.biortech.2019.122348

Maldhure, A. V., and Ekhe, J. D. (2011). "Preparation and characterizations of microwave assisted activated carbons from industrial waste lignin for Cu(II) sorption," *Chemical Engineering Journal* 168(3), 1103-1111. DOI: 10.1016/j.cej.2011.01.091

Masashi, K., Takaharu, H., Fuminori, H., and Toshimitsu, H. (2011). "Thermal conversion of alkaline lignin and its structured derivatives to porous carbonized materials," *Bioresource Technology* 102(10), 6279-6285. DOI: 10.1016/j.biortech.2011.03.023

Naseer, A., Jamshaid, A., Hamid, A., Muhammad, N., Ghauri, M., Iqbal, J., Rafiq, S., Khuram, S., and Shah, N. S. (2018). "Lignin and lignin based materials for the

removal of heavy metals from wastewater – An overview," *Zeitschrift für Physikalische Chemie* 233(3), 315-345. DOI: 10.1515/zpch-2018-1209

Reddad, Z., Zerente, C., Andres, Y., and Le, C. P. (2003). "Mechanisms of Cr(III) and Cr(VI) removal from aqueous solutions by sugar beet pulp," *Environmental Technology* 24(2) 257-264. DOI: 10.1080/09593330309385557

Sehrish, A. K., Aziz, R., Hussain, M. M., Rafiq, M. T., Rizwan, M., Muhammad, N., Rafiq, M. K., Sehar, A., Din, J. u., Al-Wabel, M. I., and Ali, S. (2019). "Effect of poultry litter biochar on chromium (Cr) bioavailability and accumulation in spinach (*Spinacia oleracea*) grown in Cr-polluted soil," *Arabian Journal of Geosciences* 12, 57. DOI: 10.1007/s12517-018-4213-z

Shan, R., Shi, Y. Y., Gu, J., Bi, J. W., Yuan, H. R., Luo, B., and Chen, Y. (2020). "Aqueous Cr(VI) removal by biochar derived from waste mangosteen shells: Role of pyrolysis and modification on its absorption process," *Journal of Environmental Chemical Engineering* 8(4), article no. 103885. DOI: 10.1016/j.jece.2020.103885

Shen, Y. S., Wang, S. L., Tzou, Y. M., Yan, Y. Y., and Kuan, W. H. (2012). "Removal of hexavalent Cr by coconut coir and derived chars – The effect of surface functionality," *Bioresource Technology* 104, 165-172. DOI: 10.1016/j.biortech.2011.10.096

Shinogi, Y., and Kanri, Y. (2003). "Pyrolysis of plant, animal and human waste: Physical and chemical characterization of the pyrolytic products," *Bioresource Technology* 90 (3), 241-247. DOI: 10.1016/s0960-8524(03)00147-0

Tariq, M. A., Nadeem, M., Iqbal, M. M., Imran, M., Siddique, M., Iqbal, Z., Amjad, M., Rizwan, M., and Ali, S. (2020). "Effective sequestration of Cr (VI) from wastewater using nanocomposite of ZnO with cotton stalks biochar: Modeling, kinetics, and reusability," *Environmental Science and Pollution Research* 27, 33821-33834. DOI: 10.1007/s11356-020-09481-x

Wang, W., Wang, X. J., Wang, X., Yang, L. Z., Wu, Z., Xia, S. Q., and Zhao, J. F. (2013). "Cr(VI) removal from aqueous solution with bamboo charcoal chemically modified by iron and cobalt with the assistance of microwave," *Journal of Environmental Sciences* 25 (9), 1726-1735. DOI: 10.1016/s1001-0742(12)60247-2

Wang, R. Z., Huang, D. L., Liu, Y. G., Zhang, C., Lai, C., Zeng, G. M., Cheng, M., Gong, X. M., Wan, J., and Luo, H. (2018). "Investigating the adsorption behavior and the relative distribution of Cd^{2+} sorption mechanisms on biochars by different feedstock," *Bioresource Technology* 261, 265-271. DOI: 10.1016/j.biortech.2018.04.032

Wang, A. Q., Zheng, Z. K., Li, R. Q., Hu, D., Lu, Y. R., Luo, H. X., and Yan, K. (2019). "Biomass-derived porous carbon highly efficient for removal of Pb(II) and Cd(II)," *Green Energy & Environment* 4(4), 414-423. DOI: 10.1016/j.gee.2019.05.002

Wang, H. X., Zhang, M. L., and Lv, Q. (2019). "Removal efficiency and mechanism of Cr(VI) from aqueous solution by maize straw biochars derived at different pyrolysis temperatures," *Water* 11(4), 781. DOI: 10.3390/w11040781

Wang, H., Yang, N. C., and Qiu, M. Q. (2020). "Adsorption of Cr(VI) from aqueous solution by biochar-clay derived from clay and peanut shell," *Journal of Inorganic Materials* 35(3), 301-308. DOI: 10.15541/jim20190350

Yang, Y. Q., Chen, N., Feng, C. P., Li, M., and Gao, Y. (2018). "Chromium removal using a magnetic corncob biochar/polypyrrole composite by adsorption combined with reduction: Reaction pathway and contribution degree," *Colloids and Surfaces A: Physicochemical and Engineering Aspects* 556, 201-209. DOI:

10.1016/j.colsurfa.2018.08.035

Yang, T., Han, C. Y., Tang, J., and Luo, Y. M. (2020). "Removal performance and mechanisms of Cr(VI) by an in-situ self-improvement of mesoporous biochar derived from chicken bone," *Environmental Science and Pollution Research* 27, 5018-5029. DOI: 10.1007/s11356-019-07116-4

Yousef, R. I., El-Eswed, B., and Al-Muhtaseb, A. A. H. (2011). "Adsorption characteristics of natural zeolites as solid adsorbents for phenol removal from aqueous solutions: Kinetics, mechanism, and thermodynamics studies," *Chemical Engineering Journal* 171(3), 1143-1149. DOI:10.1016/j.cej.2011.05.012

Zhang, X. F., Zhang, X. H., and Chen, Z. G. (2017). "Biosorption of Cr(VI) from aqueous solution by biochar derived from the leaf of *Leersia hexandra* Swartz," *Environmental Earth Sciences* 76, 67. DOI: 10.1007/s12665-016-6336-4

Zhang, X., Fu, W. J., Yin, Y. X., Chen, Z. H., Qiu, R. L., Simonnot, M. O., and Wang, X. F. (2018). "Adsorption-reduction removal of Cr(VI) by tobacco petiole pyrolytic biochar: Batch experiment, kinetic and mechanism studies," *Bioresource Technology* 268, 149-157. DOI: 10.1016/j.biortech.2018.07.125

Zibaei, Z., Ghasemi-Fasaei, R., Ronaghi, A., Zarei, M., and Zeinali, S. (2020). "Improvement of biochar capability in Cr immobilization *via* modification with chitosan and hematite and inoculation with *Pseudomonas putida*," *Communications in Soil Science and Plant Analysis* 51(7), 963-975. DOI: 10.1080/00103624.2020.1744624

Article submitted: April 16, 2021; Peer review completed: June 7, 2021; Revised version received and accepted: July 22, 2021; Published: July 29, 2021.
DOI: 10.15376/biores.16.3.6363-6377